Visualizable Cylindrical Macromolecules with Controlled Stiffness from Backbones Containing Libraries of Self-Assembling Dendritic Side Groups

V. Percec,*,† C.-H. Ahn,† W.-D. Cho,† A. M. Jamieson,† J. Kim,† T. Leman,† M. Schmidt,‡ M. Gerle,‡ M. Möller,§ S. A. Prokhorova,§ S. S. Sheiko,§ S. Z. D. Cheng,|| A. Zhang,|| G. Ungar,⊥ and D. J. P. Yeardley⊥

Contribution from The W. M. Keck Laboratories for Organic Synthesis, Department of Macromolecular Science, Case Western Reserve University, Cleveland, Ohio 44106-7202, Institut für Physikalische Chemie, Johannes Gutenberg-Universität, Jakob-Welder-Weg 11, D-55128 Mainz, Germany, Organische Chemie II, Makromolekulare Chemie, Universität Ulm, D-89069 Ulm, Germany, Maurice Morton Institute of Polymer Science, University of Akron, Akron, Ohio 44325-3909, and Department of Engineering Materials and Center for Molecular Materials, University of Sheffield, Sheffield S1 3JD, U.K.

Received April 10, 1998

Abstract: The synthesis and structural analysis of a library containing 13 taper- and conical-shaped self-assembling dendrons, 16 dendritic monomers, and their corresponding polymers is reported. Fifteen of these polymers exhibit a well-defined cylindrical shape produced by the self-assembly of their dendritic side groups that self-organizes in a hexagonal columnar two-dimensional liquid crystalline lattice. The retrosynthetic analysis of this lattice by X-ray diffraction (XRD) showed that the diameter (60 to 41 Å) and the number of repeat units forming the cylinder cross-section (7 to 1.9) of these polymers are determined by the structure of their dendritic side groups. This demonstrates that, in the hexagonal columnar lattice, the conformation (from helical to fully extended) and the stiffness of the polymer backbone penetrating through the center of the cylinder are controlled in a systematic and predictive way by the structure of the side groups. Dynamic and static light-scattering experiments have demonstrated the same trend for the stiffness of these polymers in solution (Kuhn segment length from 200 to 1032 Å). Single chains and monolayers of these polymers were visualized and quantitatively analyzed by scanning force microscopy (SFM) on a graphite surface to provide the first comparative study of the conformation, stiffness, and contour length in solution (by light scattering), in the disordered solid state on a flat substrate (by SFM), and in the hexagonal columnar lattice (by XRD). The elaboration of this library of visualizable cylindrical macromolecules with controlled chain conformation and stiffness accesses the elucidation of many fundamental problems of the field of polymer science at the molecular level and the design of multifunctional nanoscale systems based on single polymer chains.

Introduction

Our present knowledge on the shape, size, and conformation of flexible, semiflexible, and rigid synthetic macromolecules in crystalline, liquid crystalline, and amorphous states, as well as in solution, was obtained by interpreting various scattering results generated by sources such as X-rays, electrons, light, laser, and neutrons (Chart 1).[1] This was due to the very small size, particularly the diameter (several angstroms), of the backbone of synthetic macromolecules. *By contrast, biological macromolecules have benefited from their direct visualization with a resolution that allowed the most detailed analysis of the complex topology or architecture of the individual molecules. This was accomplished by a complexation process that thickened their diameter to values that permitted the desired resolution (about 50 Å).* Although in most instances direct visualization via microscopy techniques is only complementary to scattering methods, there are many examples where it played a most significant role.

The impact of quantitative analysis via direct *visualization*[2] of individual macromolecules in a lattice or amorphous state

† Case Western Reserve University.
‡ Johannes Gutenberg-Universität.
§ Universität Ulm.
|| University of Akron.
⊥ University of Sheffield.

(1) (a) Flory, P. J. *Statistical Mechanics of Chain Molecules*; Hanser: New York, 1989. (b) Keller, A.; Goldbeck, G. Polymer Crystallization: Fundamentals of Structure and Crystal Growth of Flexible Chains. In *Comprehensive Polymer Science*, 2nd Suppl.; Allen, G., Ed.; Elsevier: Oxford, 1996; pp 241−305. (c) Higgins, J. S.; Benoit, H. C. *Polymers and Neutron Scattering*; Clarendon Press: Oxford, 1994. (d) Pecora, R., Ed. *Dynamic Light Scattering. Application of Photon Correlation Spectroscopy*; Plenum Press: New York, 1985. (e) Brown, W., Ed. *Dynamic Light Scattering*; Clarendon Press: Oxford, Vol. 1, 1993; Vol. 2, 1996. (f) Chu, B. *Laser Light Scattering*, 2nd ed.; Academic Press: New York, 1991. (g) Strobl, G. *The Physics of Polymers*; Springer-Verlag: Berlin, 1996. (h) Grosberg, A. Y.; Khokhlov, A. R. *Giant Molecules*; Academic Press: New York, 1997. (i) Morawetz, H. *Macromolecules in Solution*, 2nd ed.; Wiley: New York, 1975.

(2) (a) For biochemical topology, see: Wasserman, S. A.; Cozzarelli, W. R. *Science* **1986**, *232*, 951. (b) For chemical topology, see: Walba, D. M. *Tetrahedron* **1985**, *41*, 3161. (c) In this article, *visualization* does not mean only the imaging of a structure by a microscopic technique such as SFM in a 2-D crystal or TEM in a 3-D crystal as reported repeatedly (see ref 35). Instead, by analogy with the *visualization* of the DNA (refs 2, 3) topology, we mean the quantitative analysis of a single polymer chain, i.e., diameter, contour length, end-to-end contacts, nodes, overlay at the crossing points, etc., in both ordered and disordered states. With the present microscopic methodologies, this requires a chain thickness of about 50 Å.

S0002-7863(98)01211-6 CCC: $15.00
Published on Web 08/15/1998

Chart 1. Conformation of Flexible and Semiflexible Macromolecules in Amorphous, Melt, Solution (Random-Coil for All, See a), Crystalline (Lamellar, See b), and Liquid Crystalline (Extended, See c) States and of Rigid and Semirigid Macromolecules (Wormlike, See d)

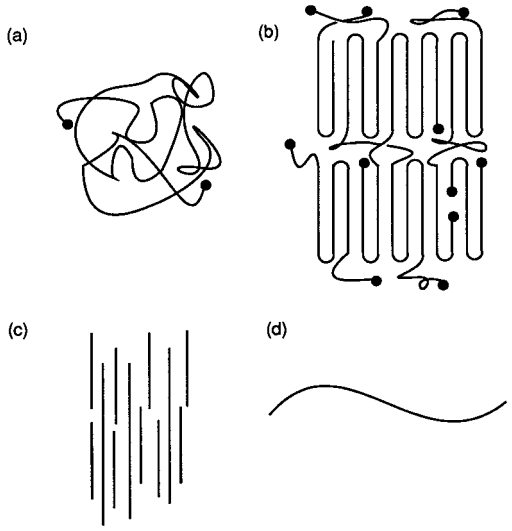

and of single molecules in two and three dimensions on the evolution of biological macromolecular science will be illustrated by two examples. The first one is the development of biochemical topology.[2] The only technique for the direct and complete topological analysis of circular DNA stereoisomers and enantiomers based on catenanes, knots, etc. was generated by coating[3] the nucleic acid with proteins via complexation. The resulting complex is stiffer and has a thicker diameter (about 50−100 Å) than the uncomplexed DNA. This treatment allowed direct visualization and quantitative analysis by transmission electron microscopy (TEM)[2,3] to reliably determine the signs of nodes, the relative direction, and the overlay and underlay at the crossing points of single molecules of circular DNA. A second significant impact was provided by the direct visualization and subsequent classification of another class of complexes of nucleic acids with protein coats,[4] i.e., helical and icosahedral viruses.[5]

Recently,[6] we proposed a strategy for the systematic design and synthesis of macromolecules with controlled backbone conformation, shape (i.e., spherical and cylindrical), and size, including diameter, by a covalent coating[6] of conventional polymer backbones with dendritic side groups which self-assemble into spherical or cylindrical supramolecular dendrimers. This strategy is outlined in Chart 2 and allows the systematic construction of well-defined synthetic macromolecules with diameters sufficiently thick (about 50 Å) for direct visualization and quantitative analysis of single molecules in two dimensions by scanning force microscopy (SFM)[6] and in three dimensions by TEM.[7]

Chart 2. Natural and Synthetic Supramolecular Systems with Cylindrical and Shperical Shapes: (a) Tobacco Mosaic Virus, (b) Icosahedral Virus, Synthetic Analogue of a and b Self-Assembled from Tapered (c) and Conical (d) Monodendrons Containing Endo Receptors or Polymer Backbones as X Groups and Their Subsequent Self-Organization in P6mm Φ_h and $Pm\bar{3}n$ Cubic Lattices, Respectively[a]

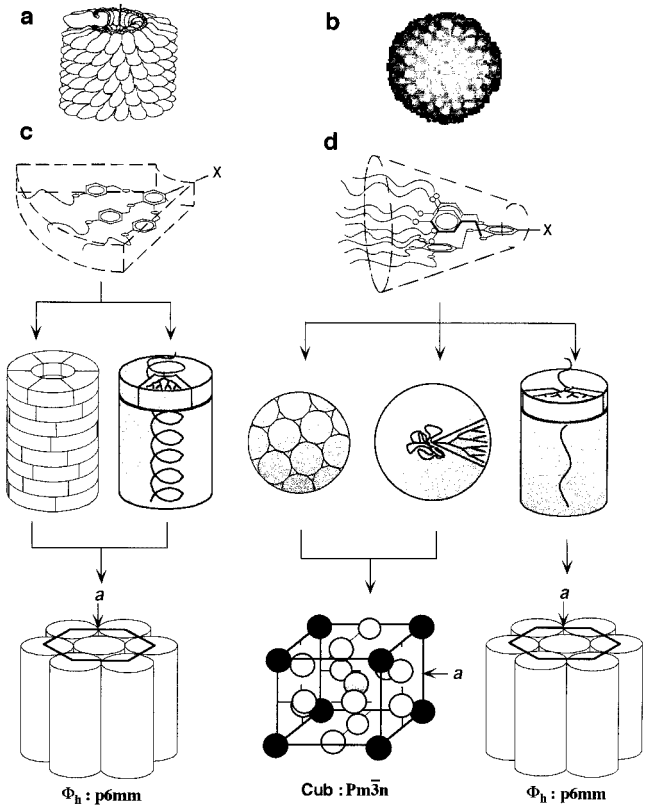

[a] For more details, see refs 6, 7, 10, 12.

In our strategy (Chart 2), the natural self-assembling protein building blocks have been substituted with monodendrons[6,7,8k] of similar shapes. Monodendrons[8a,b,d,j,k,9d] and dendrimers[8a−d,j,9] have been shown to represent some of the most powerful synthetic building blocks that can be employed in the construction of supramolecular and macromolecular systems with well-

(3) (a) Krasnow, M. A.; Stasiak, A.; Spengler, S. J.; Dean, F.; Koller, T.; Cozzarelli, N. R. *Nature* **1983**, *304*, 559. (b) Wasserman, S. A.; Dungan, J. M.; Cozzarelli, N. R. *Science* **1985**, *229*, 171. (c) For a review, see: Chambron, J.-C.; Dietrich-Buchecker, C.; Sauvage, J.-P. In *Comprehensive Supramolecular Chemistry*; Lehn, J.-M., Ed.; Elsevier: Oxford, 1997; Vol. 9, pp 43−83. (d) *Dendritic coat* and *coating* are terms transplanted from molecular biology. A *protein coat* represents an assembly of proteins into a cage or a protective coat that surrounds the nucleic acid of a virus and protects it from being altered by the environment. Dendritic coat has a similar meaning as protein coat (see also ref 4).

(4) (a) Klug, A. *Angew. Chem., Int. Ed. Engl.* **1983**, *22*, 565. (b) Levine, A. J. *Viruses*; Freeman: New York, 1995. (c) Stryer, L. *Biochemistry*; Freeman: New York, 1988; p 85.

(5) Ackermann, A. W.; Berthiaume, L. *Atlas of Virus Diagrams*; CRC: New York, 1995.

(6) Percec, V.; Ahn, C.-H.; Ungar, G.; Yeardley, D. J. P.; Möller, M.; Sheiko, S. *Nature (London)* **1998**, *391*, 161.

(7) Hudson, S. D.; Jung, H.-T.; Percec, V.; Cho, W.-D.; Johansson, G.; Ungar, G.; Balagurusamy, V. S. K. *Science* **1997**, *278*, 449.

(8) (a) Fréchet, J. M. J. *Science* **1994**, *263*, 1710. (b) Tomalia, D. A.; Durst, H. D. *Top. Curr. Chem.* **1993**, *165*, 193. (c) Newkome, G. R.; Moorefield, C. N.; Vögtle, F. *Dendritic Molecules. Concepts, Synthesis, Perspectives*; VCH: Weinheim, 1996. (d) Moore, J. S. *Acc. Chem. Res.* **1997**, *30*, 402. (e) Percec, V.; Chu, P.; Ungar, G.; Zhou, J. *J. Am. Chem. Soc.* **1995**, *117*, 11441. (f) Knapen, J. W. J.; van der Made, A. W.; de Wilde, J. C.; van Leeuwen, P. W. N.; Wijkens, P.; Grove, D. M.; van Koten, G. *Nature* **1994**, *372*, 659. (g) van Hest, J. C. M.; Delnoye, D. A. P.; Baars, M. W. P. L.; van Genderen, M. H. P.; Meijer, E. W. *Science* **1995**, *268*, 1592. (h) McElhanon, J. R.; McGrath, D. V. *J. Am. Chem. Soc.* **1998**, *120*, 1647. (i) Jiang, D.-L.; Aida, T. *Nature* **1997**, *378*, 454. (j) Tomalia, D. A. *Adv. Mater.* **1994**, *6*, 529. (k) *Monodendron:* a single dendron synthesized by the convergent approach (see refs 8a−c, 9).

(9) (a) Hawker, C.; Fréchet, J. M. J. *J. Am. Chem. Soc.* **1990**, *112*, 7638. (b) Miller, T. M.; Neenan, T. X. *Chem. Mater.* **1990**, *2*, 346. For brief reviews, see: (c) Hawker, C. J.; Wooley, K. L. In *Advances in Dendritic Macromolecules*; Newkome, G. R., Ed.; JAI Press: Greenwhich, CT, 1995; Vol. 2, p 1. (d) Fréchet, J. M. J.; Hawker, C. J. In *Comprehensive Polymer Science*, 2nd Suppl.; Allen, G., Ed.; Elsevier: Oxford, 1996; pp 71−132.

defined shapes and size controllable at the angstrom level.[8,9] Simultaneously, nucleic acids have been substituted with conventional synthetic macromolecules.[6]

A convergent[9] methodology has been elaborated for the construction of flat taper[10]-shaped monodendrons (Chart 2c) that self-assemble into cylindrical supramolecular dendrimers. These cylindrical supramolecular dendrimers self-organize in a hexagonal columnar (Φ_h) two-dimensional (2-D) p6mm lattice.[7,10] Retrosynthetic analysis of the p6mm Φ_h lattice by X-ray diffraction (XRD) allows the determination of the internal structure of the individual supramolecular columns and of the shape and size of its monodendritic building blocks.[10] The attachment of a polymerizable group to the flat tapered monodendron, followed by polymerization, yields a cylindrical polymer with a helical chain penetrating through its center and having a pitch determined by the number of monodendrons that generates a column stratum of constant height.[11] Therefore, the number of monodendrons in a column cross-section of constant height determines the conformation of the polymer backbone penetrating through its center (Chart 2).[6,11]

Increasing the number of alkyloxy substituents of the benzyl ether groups on the periphery of the AB_3 monodendron, from one in the para position to two or three placed in the 3,4 or 3,4,5 positions (Chart 2d), changes the overall shape of the monodendron from flat tapered[7,10] into conical.[12] Conical monodendrons[12] self-assemble into spherical supramolecular dendrimers which self-organize in a three-dimensional (3-D) $Pm\bar{3}n$ cubic liquid crystalline (LC) lattice (Chart 2d).[7,12] Retrosynthetic XRD analysis of the $Pm\bar{3}n$ unit cell gives details on the shape, size, and number of monodendrons that form a supramolecular spherical dendrimer.[12]

In a preliminary communication,[6] we demonstrated that polymerization of conical monodendritic monomers yields, up to a degree of polymerization (DP) that approximately corresponds to the number of monodendrons which form a supramolecular spherical dendrimer, spherical macromolecules containing their random-coil backbone confined to their core (Chart 2d).[6] Above this degree of polymerization, due to the "quasi-equivalence" [6] of these conformationally flexible monodendrons, they get distorted into a flat tapered shape, and the resulting macromolecule adopts a cylindrical shape, with its extended backbone penetrating through its center.[6] XRD analysis of the $Pm\bar{3}n$ and p6mm lattices provides information on the internal structure of the object-like well-defined spherical[6] and cylindrical[6,11,13] polymers. These 2-D and 3-D lattices were imaged by SFM[6] on a surface in two dimensions and by TEM[7] in three dimensions. The self-assembly and self-organization in LC lattices ensures a thermodynamic control for both processes.[7,10,12,14,15]

The potential impact of a class of synthetic cylindrical macromolecules with controlled stiffness, diameter, architecture, and topology that can be analyzed quantitatively at the molecular level via various visualization techniques in the same manner as complexed thickened DNA chains,[2−5] to the field of polymer science, can be as high as or even higher than that of visualizable natural macromolecules and their complex systems to the field of biology.

Toward this goal, we have designed the first library of self-assembling monodendritic monomers and their corresponding polymers. The synthesis of the first and second generation of monodendritic monomers and polymers from this library and the analysis of the polymers in solid and Φ_h states by XRD, and in solution by dynamic and static light scattering, as well as their direct visualization and quantitative analysis as single chains and as monolayers on a surface by SFM, are reported in this publication. These experiments were facilitated by the controlled radical polymerization of monodendritic monomers in the self-assembled state.[6,16] Methodologies based on uncontrolled radical[9d,11,13,17−20] and living metathesis[11a,b,21] polymerizations require long reaction times and provide only a limited range of polymer molecular weights.

Results and Discussion

Synthesis of the Monodendritic Library of Monomers. Chart 3 outlines the structures of the first library of taper- and cone-shaped monodendritic styrene and methacrylate monomers and of their corresponding polymers. The short nomenclature used in Chart 3 is explained in Chart 4. All monodendritic monomers were synthesized according to methods reported previously from our laboratory for ***(3,4,5−3,4,5)*12G2-X**, where X was CO_2CH_2S, CO_2CH_2PS, CH_2MA, and CH_2PMA.[6,12,16] Their detailed synthesis and structural characterization is provided in the Supporting Information.

Radical Polymerization of Monodendritic Monomers. In a preliminary communication,[16] we reported that, above a critical monodendritic monomer concentration, self-assembly produces a self-encapsulation of the polymerizable groups in a reactor that is generated by jacketing the polymerizable groups with their own supramolecular dendritic coat.[6] This self-encapsulation accelerates the polymerization process which, in combination with a low rate constant of termination determined by steric hindrance, generates a controlled radical polymerization. By contrast, radical polymerization of monodendritic monomers which do not self-assemble either does not yield polymers[19] or produces high-molecular-weight polymers in ideal solution[19c,20] or in melt[19c] only from monodendrons containing a flexible spacer and after very long reaction times. Since all monoden-

(10) (a) Percec, V.; Johansson, G.; Ungar, G.; Zhou, J. *J. Am. Chem. Soc.* **1996**, *118*, 9855. (b) *Tapered monodendron*: a monodendron with a shape similar to that of a slice of pizza or a slice of cake (see Chart 2c).

(11) (a) Percec, V.; Schlueter, D. *Macromolecules* **1997**, *30*, 5783. (b) Percec, V.; Schlueter, D.; Ronda, J. C.; Johansson, G.; Ungar, G.; Zhou, J. P. *Macromolecules* **1996**, *29*, 1464. (c) Kwon, Y. K.; Chvalun, S. N.; Blackwell, J.; Percec, V.; Heck, J. *Macromolecules* **1995**, *28*, 1552. (d) Kwon, Y. K.; Chvalun, S. N.; Schneider, A. I.; Blackwell, J.; Percec, V.; Heck, J. *Macromolecules* **1994**, *27*, 6129. (e) Kwon, Y. K.; Danko, C.; Chvalun, S. N.; Blackwell, J.; Heck, J.; Percec, V. *Macromol. Symp.* **1994**, *87*, 103.

(12) (a) Balagurusamy, V. S. K.; Ungar, G.; Percec, V.; Johansson, G. *J. Am. Chem. Soc.* **1997**, *119*, 1539. (b) *Conical monodendron*: see Chart 3d and refs 6, 7, 12a, 16.

(13) (a) Percec, V.; Schlueter, D.; Ungar, G.; Cheng, S. Z. D.; Zhang, A. *Macromolecules* **1998**, *31*, 1745. (b) Johansson, G.; Percec, V.; Ungar, G.; Zhou, J. P. *Macromolecules* **1996**, *29*, 646. (c) Percec, V.; Schlueter, D.; Kwon, Y. K.; Blackwell, J.; Moeller, M.; Slangen, P. J. *Macromolecules* **1995**, *28*, 8807.

(14) (a) de Gennes, P. G. *Angew. Chem., Int. Ed. Engl.* **1992**, *31*, 842. (b) de Gennes, P. G.; Prost, J. *The Physics of Liquid Crystals*; Oxford University Press: Oxford, 1993. (c) Percec, V. In *Handbook of Liquid Crystal Research*; Collings, P. J., Patel, J. S., Eds.; Oxford University Press: Oxford, 1997; pp 259−346.

(15) Lehn, J.-M. *Supramolecular Chemistry*; VCH: Weinheim, 1995.

(16) Percec, V.; Ahn, C.-H.; Barboiu, B. *J. Am. Chem. Soc.* **1997**, *119*, 12978.

(17) Percec, V.; Schlueter, D.; Kwon, Y. K.; Blackwell, J.; Möller, M.; Slangen, P. J. *Macromolecules* **1995**, *28*, 8807.

(18) Percec, V.; Schlueter, D.; Ungar, G.; Cheng, S. Z. D.; Zhang, A. *Macromolecules* **1998**, *31*, 1745.

(19) (a) Draheim, G.; Ritter, H. *Macromol. Chem. Phys.* **1995**, *196*, 2211. (b) Chen, Y.-M.; Chen, C.-F.; Li, Y.-F.; Xi, F. *Macromol. Rapid. Commun.* **1996**, *17*, 401. (c) Neubert, I.; Klopsch, R.; Claussen, W.; Schlueter, A.-D. *Acta Polym.* **1996**, *47*, 455.

(20) (a) Percec, V.; Heck, J.; Tomazos, D.; Falkenberg, F.; Blackwell, H.; Ungar, G. *J. Chem. Soc., Perkin Trans. 1* **1993**, 2799. (b) Percec, V.; Schlueter, D. *Macromolecules* **1997**, *30*, 5783.

(21) Stewart, G. M.; Fox, M. A. *Chem. Mater.* **1998**, *10*, 860.

Chart 3. Structures of the Monodendritic Monomers, Their Corresponding Polymers, and Summary of the Self-Organization of the Library of Cylindrical Macromolecular Dendrimers and of Their Retrosynthetic Analysis by XRD (a = Lattice Parameter Equal to Cylinder Diameter in Φ_h Phase or Two Times the Sphere Diameter in the Cubic Phase; μ = Number of Monodendrons in a Cylinder Cross-Section of 3.74 Å Height or in a Spherical Supramolecular Dendrimer

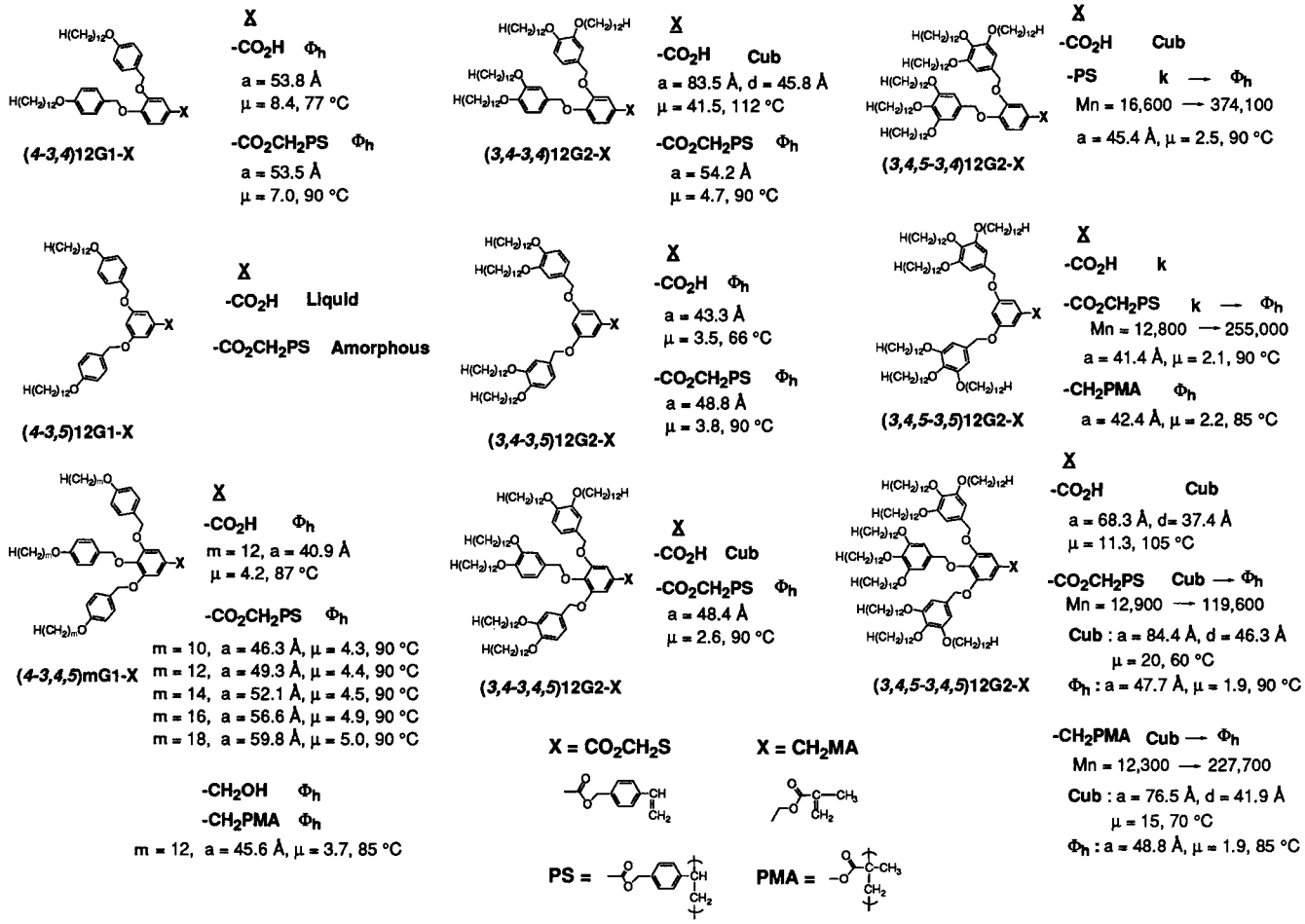

Chart 4. Short Nomenclature for Monodendrons

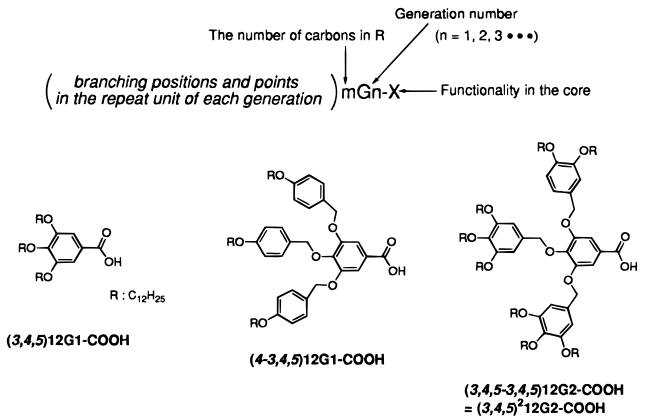

dritic monomers discussed here self-assemble either in cylindrical or spherical supramolecular dendrimers, their radical polymerization was controlled as described previously.[16] Table 1 summarizes the polymerization conditions and results, including relative number-average molecular weights (M_n(rel, PS)) obtained by SEC with polystyrene standards as well as M_w/M_n-(rel, PS) values. *As in the previous case,*[16] *high-molecular-weight polymers were obtained within less than 5 min reaction time when the polymerization was performed in bulk or in solution above the critical monomer concentration.* Therefore, this controlled polymerization reaction is more convenient than living methathesis polymerization of monodendritic monomers.[11a,b,21] The M_n(rel, PS) values reported in Table 1 are from 2 to 5 times lower than the absolute values obtained by light scattering (to be discussed later).

Analysis of Polymer Shape in Solid State by a Combination of DSC, XRD, and Thermal Optical Polarized Microscopy. The 2-D hexagonal columnar (Φ_h) LC lattice self-organized from cylindrical macromolecules was identified by a combination of DSC and thermal optical polarized microscopy.[10] The retrosynthetic analysis of the 2-D Φ_h lattice by XRD provided the lattice parameter (a, Chart 2) and the number of dendritic building blocks generating a stratum of constant height of the cylinder.[10]

Figure 1 shows selected examples of DSC traces obtained from the cooling scans of **(*4*−*3,4,5*)12G1-CO_2CH_2PS** with different DP determined relative to polystyrene standards (DP_{PS}) and of **(*4*−*3,4,5*)mG1-CO_2CH_2PS** (m = 10, 12, 14, 16, 18) with the highest DP_{PS} obtained (Table 1). The first-order transition from the isotropic (i) to the Φ_h phase determined by DSC (Figure 1) was qualitatively assigned through the fan-shaped focal conic texture observed on the optical polarized microscope[10] and was confirmed by XRD.[10] An increase in the isotropization temperature of the Φ_h phase ($T_{\Phi_{h-i}}$) can be induced by an increase in the polymer molecular weight (Figure 1a), its diameter (Figure 1b), and/or its rigidity.[14c,22] Transition temperatures of polymers with various structures and molecular weights are summarized in Table 1.

Table 1. Synthesis and Characterization of PS and PMA with Monodendritic Side Groups by SEC (versus Polystyrene Standards) and by Differential Scanning Calorimetry (DSC)

monomer	$[M]_o$ (mol/L)	reaction time (h)	conversion (%)	M_n (rel, PS)	M_w/M_n (rel, PS)	DP_{PS}	thermal transitions (°C) and corresponding enthalpy changes (kcal/mol) heating	cooling
(*4*−*3,4*)12G1-CO_2CH_2S	0.40[a]	24	82.1	9 600	1.58	11.7	Φ_h 124(0.23) i	i 117(0.12) Φ_h
	0.65[b]	5	74.0	58 400	2.97	71.3	Φ_h 155(0.31) i	i 147(0.31) Φ_h
(*4*−*3,5*)12G1-CO_2CH_2S	0.42[a]	24	81.6	16 600	1.36	20.3	amorphous	
	1.22[b]	0.08	39.1	326 100	2.24	398.1	amorphous	
(*4*−*3,4,5*)10G1-CO_2CH_2S	0.49[a]	20	92.0	24 600	2.12	24.0	Φ_h 117(0.33) i	i 104(0.35) Φ_h
	0.57[a]	2	76.8	127 000	2.71	123.8	Φ_h 130(0.19) i	i 113(0.18) Φ_h
	0.98[b]	0.08	62.7	333 800	2.72	325.5	Φ_h 131(0.08) i	i 113(0.08) Φ_h
(*4*−*3,4,5*)12G1-CO_2CH_2S	0.26[a]	24	76.7	12 200	1.22	11.2	Φ_h 111(0.24) i	i 102(0.28) Φ_h
	0.37[a]	24	74.8	23 100	1.88	20.8	Φ_h 116(0.44) i	i 106(0.51) Φ_h
	0.46[a]	5	74.6	39 200	2.16	35.4	Φ_h 129(0.26) i	i 114(0.27) Φ_h
	0.55[a]	3	81.0	51 900	2.65	46.8	Φ_h 135(0.22) i	i 120(0.26) Φ_h
	0.90[b]	0.08	66.0	103 900	2.08	93.6	Φ_h 138(0.18) i	i 122(0.19) Φ_h
(*4*−*3,4,5*)12G1-CH_2MA	0.47[a]	3	95.1	177 300	4.37	169.2	Φ_h 121(0.25) i	i 117(0.22) Φ_h
	0.57[a]	0.25	93.0	288 000	2.33	274.9	Φ_h 122(0.28) i	i 120(0.26) Φ_h
(*4*−*3,4,5*)14G1-CO_2CH_2S	0.25[a]	24	51.2	11 600	1.24	9.7	k 7(4.21) Φ_h 103(0.26) i	i 92(0.24) Φ_h 1(4.53) k
	0.28[a]	24	82.0	17 200	1.33	14.4	k 9(3.52) Φ_h 119(0.32) i	i 109(0.38) Φ_h 3(3.84) k
	0.47[a]	20	85.2	40 100	2.39	33.6	k 9(8.97) Φ_h 135(0.21) i	i 119(0.36) Φ_h 3(9.91) k
	0.84[b]	0.08	57.7	284 300	2.35	238.1	k 8(8.81) Φ_h 150(0.12) i	i 130(0.19) Φ_h 2(9.17) k
(*4*−*3,4,5*)16G1-CO_2CH_2S	0.25[a]	24	71.3	13 400	1.37	10.5	k 30(8.95) Φ_h 108(0.33) i	i 98(0.36) Φ_h 22(7.94) k
	0.26[a]	24	77.1	14 300	1.25	11.1	k 29(9.35) Φ_h 113(0.45) i	i 102(0.45) Φ_h 21(9.53) k
	0.42[a]	20	85.5	46 900	1.90	36.7	k 30(8.33) Φ_h 131(0.19) i	i 118(0.24) Φ_h 22(8.24) k
	0.78[b]	0.08	38.1	114 600	2.57	89.7	k 30(14.87) Φ_h 152(0.18) i	i 134(0.16) Φ_h 22(14.32) k
(*4*−*3,4,5*)18G1-CO_2CH_2S	0.24[a]	24	64.1	14 900	1.21	11.0	k 45(12.79) Φ_h 113(0.45) i	i 103(0.42) Φ_h 36(12.06) k
	0.72[b]	0.08	71.5	188 700	3.48	138.6	k 44(11.9) Φ_h 165(0.23) i	i 139(0.06) Φ_h 36(11.3) k
(*3,4*−*3,4*)12G2-CO_2CH_2S	0.93[b]	0.08	67.8	148 900	2.28	138.2	Φ_h 290 dec	
(*3,4*−*3,5*)12G2-CO_2CH_2S	0.93[b]	0.08	66.2	110 900	2.90	102.9	Φ_h 290 dec	
(*3,4*−*3,4,5*)12G2-CO_2CH_2S	0.59[b]	0.08	32.4	127 200	2.23	74.8	Φ_h 290 dec	
(*3,4,5*−*3,4*)12G2-CO_2CH_2S	0.21[a]	24	72.9	16 600	1.30	10.7	k −18(3.14) i	i −22(3.10) k
	0.64[b]	0.08	53.9	374 100	2.22	240.3	Φ_h 290 dec	
(*3,4,5*−*3,5*)12G2-CO_2CH_2S	0.22[a]	24	61.5	12 800	1.12	8.2	k −13(3.06) i	i −19(3.43) k
	0.64[b]	0.08	50.9	255 000	2.55	163.8	Φ_h 290 dec	
(*3,4,5*−*3,5*)12G2-CH_2MA	0.67[b]	0.08	78.7	404 500	2.10	270.6	Φ_h 290 dec	
(*3,4,5*−*3,4,5*)12G2-CO_2CH_2S	0.16[a]	24	69.2	12 900	1.14	5.8	k −14(7.80) Cub 79(0.21) i	i −19(6.43) k
	0.45[b]	0.08	52.1	119 600	2.02	54.0	Φ_h 290 dec	
(*3,4,5*−*3,4,5*)12G2-CH_2MA	0.16[a]	24	78.3	12 300	1.06	5.7	k −11(7.90) Cub 82(0.19) i	i −16(6.71) k
	0.46[b]	0.08	79.1	227 700	3.11	105.7	Φ_h 290 dec	

[a] Concentration corresponds to solution polymerization at 60 °C with 1 wt % AIBN. [b] Concentration corresponds to bulk polymerization at 90 °C with 1 wt % AIBN.

Figure 2 plots the dependence of the $T_{\Phi_{h-i}}$ on DP_{PS} for the series of polymers **(*4*−*3,4,5*)mG1-CO_2CH_2PS** (m = 10, 12, 14, 16). A very clear trend is observed. In all cases, isotropization temperature increases with DP_{PS} until it reaches a plateau. However, the temperature value of this plateau increases with the increase in the number of methylenic units of the alkyloxy group from the periphery of the monodendron (m). XRD analysis of the Φ_h phase of these polymers shows that this increase is proportional with the increase in lattice parameter, *a* (*a* is equal to cylinder diameter) from 46.3 (for m = 10) to 59.8 Å (for m = 18) (bottom left side of Chart 3). A qualitative inspection of the slopes of the $T_{\Phi_{h-i}}$ on DP_{PS} (Figure 2) shows, as predicted theoretically,[14c,22] the highest slope for the **(*4*−*3,4,5*)mG1-CO_2CH_2PS** polymers with the thicker diameter (Chart 3).

A brief investigation of the results from Table 1 shows that **(*4*−*3,4*)12G1-CO_2CH_2PS**, **(*4*−*3,4,5*)mG1-CO_2CH_2PS**, and **(*4*−*3,4,5*)12G1-CH_2PMA** exhibit a transition from Φ_h to an isotopic state. **(*4*−*3,5*)12G1-CO_2CH_2PS** is amorphous (Chart 3). Increasing the number of alkyloxy substituents on the benzyl ether group from the periphery of the monodendron from one to two and respectively to three increases $T_{\Phi_{h-i}}$ to values that are higher than the decomposition temperature of the resulting polymer (290 °C) (Table 1, Chart 3). These results can be explained if we consider the number of monodendrons (μ) forming a 3.74 Å stratum of the polymeric column (Chart 3). Increasing the number of alkyloxy groups from the periphery of the monodendron decreases μ from 7.0 to 1.9. Previously, we have assigned this change in μ to a change in backbone conformation from helical (for $\mu = 7.0$ to 2.5) to fully extended (for μ about 2.0) (Chart 2).[6] This control of backbone conformation in the Φ_h state from helical to fully extended should be accompanied by an increase in the overall stiffness of the backbone of the cylindrical polymer.

Analysis of Polymer Chain Conformation in Solution by Static and Dynamic Light Scattering. Characterization of a wide range of polymers, having both PS and PMA backbones and various monodendritic side groups, was carried out by size exclusion chromatography (SEC) with both concentration and multiangle light-scattering detectors (SEC-MALLS), using THF as solvent at a flow rate of 1 mL/min.[23,24] More detailed analyses were performed on unfractionated **(*4*−*3,4,5*)12G1-CH_2PMA** and **(*4*−*3,4,5*)12G1-CO_2CH_2PS** by static and dynamic light scattering in both THF and toluene solutions.[25]

(22) (a) Percec, V.; Keller, A. *Macromolecules* **1990**, *23*, 4347. (b) Keller, A.; Ungar, G.; Percec, V. In *Advances in Liquid Crystalline Polymers*; Weiss, R. A., Ober, C. K., Eds.; ACS Symposium Series 435; Washington, DC, 1990.

(23) Wintermantel, M.; Schmidt, M.; Tsukahara, Y.; Kajiwara, K.; Kohjiva, S. *Macromol. Rapid Commun.* **1994**, *15*, 279.

(24) Wintermantel, M.; Antonietti, M.; Schmidt, M. *J. Appl. Polym. Sci., Polym. Symp.* **1993**, *52*, 91.

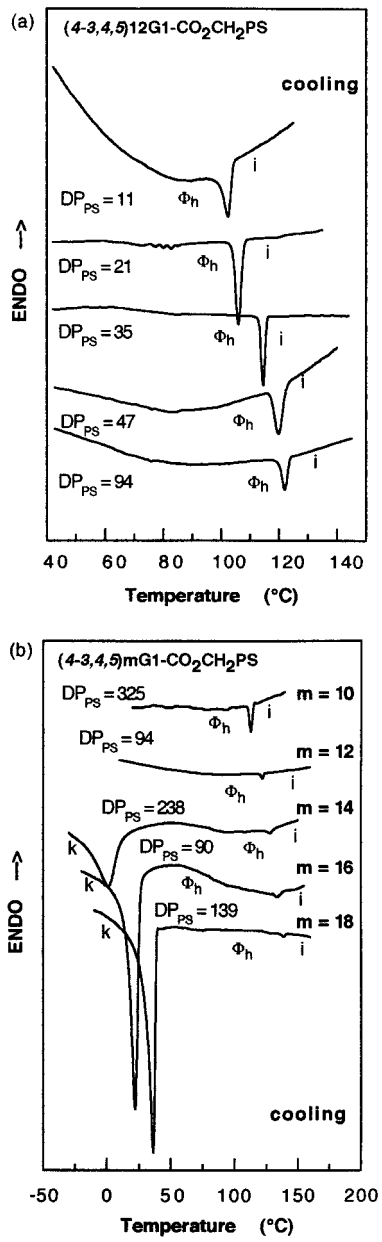

Figure 1. Cooling differential scanning calorimetric (DSC) traces of **(*4*−*3,4,5*)12G1-CO_2CH_2PS** with different degrees of polymerization relative to PS standards (DP_{PS}) (a) and of **(*4*−*3,4,5*)mG1-CO_2CH_2PS** (m = 10, 12, 14, 16, 18), with DP_{PS} shown in (b).

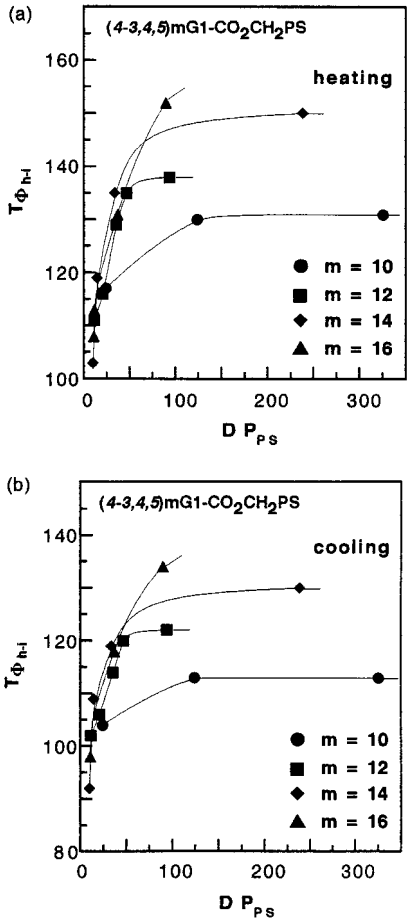

Figure 2. Dependence of the columnar hexagonal (Φ_h) isotropic (i) (Φ_{h-i}) and i−Φ_h transition temperatures of **(*4*−*3,4,5*)mG1-CO_2CH_2PS** (m = 10, 12, 14, 16) on degree of polymerization (DP_{PS}) relative to PS standards: (a) data collected from second heating and (b) from first cooling DSC scans.

SEC-MALLS studies showed anomalous elution behavior for polymer samples with *extremely high molecular weights* (see the curvature in Figure 3). In conventional size exclusion chromatography, the highest molecular weights elute at the lowest elution volume (V_e), and the radius of gyration (R_g) increases with molecular weight.[26b] Both dependences should be linear.[26b] (See Figure 3b, ◇, and Figure 7, to be discussed later). The results from Figure 3a indicate that high-molecular-weight polymers appear both at normal and at larger than expected V_e, which is inconsistent with a normal size exclusion for conventional linear polymers.[26b] The curved dependences from Figure 3 are anomalous since they provide for the same molecular weight or DP two different values of V_e and R_g. Obviously, one of the two is higher than expected. This anomalous elution leads, at extremely high molecular weight, to an anomalous nonlinear relationship when R_g determined from MALLS (see Experimental Section)[26b] is plotted against molecular weight (M_w(abs, LS)) (Figure 3b). The SEC-MALLS data[26] suggest that the anomalous eluting species with extremely high molecular weight exhibit R_g values larger than those of normally eluting species having the same M_w(abs, LS). Such an anomalous eluting behavior has been observed for polystyrene microgels and other branched polymers.[26] The present data support the conclusion of ref 26, that the extremely high molar mass fraction of the sample interacts with the column material (i.e., gets trapped) and elutes at higher elution volumes than expected by a separation mechanism based on pure size exclusion. Thus, the normally eluting macromolecules (separated by size exclusion) coelute with a small fraction of retarded, extremely high molar mass polymers. The observed anomaly is explained in the following way. At small elution volumes, the normal size exclusion separation mechanism prevails, and the polydispersity within small enough elution "slices" is negligibly small. At higher elution volumes, the normally eluting small polymers coelute with the retarded high-molecular-mass polymers, and this increases the polydispersity within an elution "slice" to values that can reach $M_w/M_n > 100$! Since the *z*-average mean-square radius of gyration increases more strongly with polydispersity than the weight-average molar mass,[26b] an upturn of the R_g-M curves results as experimentally observed. The fact that the anomaly was first observed for microgels does not mean that the present samples may contain

(25) Gu, D.; Jamieson, A. M.; Rosenblatt, C.; Tomazos, D.; Lee, M.; Percec, V. *Macromolecules* **1991**, *24*, 2385.

(26) (a) Johann, C.; Kilz, P. *J. Appl. Polym. Sci.: Appl. Polym. Symp.* **1991**, *48*, 111. (b) Wyatt, P. J. *Anal. Chim. Acta* **1993**, *272*, 1.

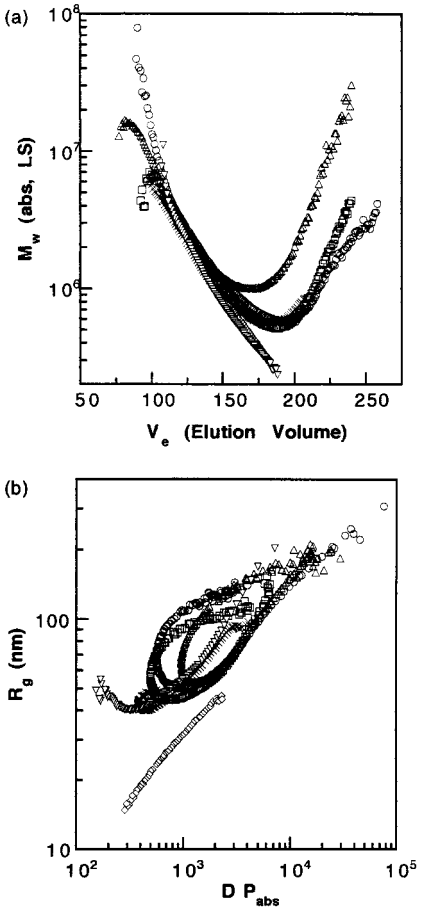

Figure 3. Dependence of the absolute weight-average molecular weight M_w(abs, LS) on elution volume (V_e) (a) and of the radius of gyration (R_g) on DP_{abs} (b); □, ○, △, ***(4−3,4,5)*12G1-CH$_2$PMA**; ◇, ***(4−3,4,5)*-12G1-CO$_2$CH$_2$PS** (see Experimental Section and ref 26b for calculations).

branched structures or aggregates, as convincingly demonstrated by the SFM pictures discussed below, by the perfection of the columnar hexagonal lattice analyzed by XRD, and by dynamic light-scattering experiments. In the following we confine the discussion and the calculations to the normally eluting samples (i.e., below the molecular weight where this anomaly is observed), as indicated by the shape of the M_w-V_e curves or R_g-DP curves (see Figure 7) and by a quantitative agreement with independent static and dynamic light-scattering experiments (Table 3).

We will describe here the R_g-M_w(abs, LS) results obtained by SEC-MALLS for the polymers ***(4−3,4,5)*12G1-CH$_2$PMA** (Figure 4a) and ***(4−3,4,5)*12G1-CO$_2$CH$_2$PS** (Figure 4b). Zimm plots[26b] by static and dynamic light-scattering analysis on unfractionated ***(4−3,4,5)*12G1-CO$_2$CH$_2$PS** and ***(4−3,4,5)*12G1-CH$_2$PMA** specimens are shown in Figure 5. Graphical analysis of Zimm plots[26b] yields, via eq 3, values of M_w(abs, LS) and $R_{g,z}$. Figure 6 presents the concentration dependence of the *z*-average translational diffusion coefficient, measured from the first cumulant of the dynamic light-scattering correlation function over the temperature range 25−50 °C. Extrapolation of these data to zero concentration provides the limiting value, $D_{t,z}^0$, from which the corresponding estimate of the hydrodynamic radius, R_h, is obtained. For ***(4−3,4,5)*12G1-CH$_2$PMA**, we obtained M_w(abs, LS) = 3.49 × 10^6, $R_{g,z}$ = 797 Å, and R_h = 504 Å. These values are numerically very consistent with the R_g-M_w(abs, LS) relationship in Figure 4a. Likewise, we obtained M_w(abs, LS) = 4.17 × 10^5, $R_{g,z}$ = 190 Å, and R_h = 148 Å for ***(4−3,4,5)*12G1-CO$_2$CH$_2$PS**, again very consistent with the R_g-M_w(abs, LS) data in Figure 4b.

First, it is interesting to contrast the measured M_w(abs, LS) = 3.49 × 10^6, $R_{g,z}$ = 797 Å, and R_h = 504 Å with R_g and R_h values estimated for a poly(methyl methacrylate) (PMMA) coil of equivalent degree of polymerization, DP_{abs} = 3245. Using literature relationships for PMMA in acetone (R_g (Å) = 0.1122$M^{0.6}$ and R_h (Å) = 0.072$M^{0.57}$),[27] we estimate R_g = 210 Å and R_h = 135 Å. The large increase in R_g and R_h for ***(4−3,4,5)*12G1-CH$_2$PMA** indicates that the PMMA backbone of ***(4−3,4,5)*12G1-CH$_2$PMA** is highly extended due to the strong steric repulsive interactions of the pendant dendritic side groups.

A similar effect is found when comparing R_g and R_h of ***(4−3,4,5)*12G1-CO$_2$CH$_2$PS** with the corresponding values for a PS chain of the same DP_{abs}. Thus, for ***(4−3,4,5)*12G1-CO$_2$CH$_2$PS**, we determine M_w(abs, LS) = 4.17 × 10^5, $R_{g,z}$ = 190 Å, and R_h = 148 Å. From the literature values for PS in toluene, R_g (Å) = 0.1185$M^{0.6}$ and R_h (Å) = 0.072$M^{0.58}$;[28] for a polystyrene (PS) coil of DP_{abs} = 376, we calculate R_g = 67 Å and R_h = 31 Å. Again, the large increase in R_g and R_h for ***(4−3,4,5)*12G1-CO$_2$CH$_2$PS** indicates the PS backbone of ***(4−3,4,5)*12G1-CO$_2$CH$_2$PS** is highly extended due to the strong steric repulsive interactions of the pendant dendritic side groups. To obtain a quantitative interpretation in terms of the chain structure, we need to investigate the molecular weight dependence of R_g for samples of narrow polydispersity, which can be performed using SEC-MALLS analysis (Figures 3 and 4a).[24,26b] Following the procedures of Wintermantel et al.,[29] these data can be fit to the expression for the radius of gyration[1a,h,i,8c] of a wormlike chain:[30]

$$R_g^2 = (aL/3)\{1 - (3a/L)[1 - (2a/L) + (2a^2/L^2) - 2(a/L)^2 \exp(-L/a)]\} \quad (1)$$

where *a*, the persistence length,[1a,g,h] is equal to one-half the Kuhn statistical segment length, l_k, and is a measure of chain stiffness, while *L* is the contour length of the chain. In these analyses, a fully extended all-trans monomer segment length $l_{monomer}$ = 2.5 Å was assumed, from which the contour length *L* is computed as $L = DP_{abs} l_{monomer}$. The resulting fits to eq 1 are shown in Figures 3 and 4 and yield, for ***(4−3,4,5)*12G1-CH$_2$PMA**, l_k = 474 Å, and for ***(4−3,4,5)*12G1-CO$_2$CH$_2$PS**, l_k = 265 Å. If the backbone has a helical conformation as it does in the solid state, $l_{monomer}$ and, correspondingly, *L* would each be smaller, and fits to eq 1 would yield larger values of the persistence length, i.e., the stiffness of the polymer backbone would be higher.

It is interesting to make a comparison with recent literature results on other polymers with bulky side groups. First, we consider the light-scattering study by Wintermantel et al.[29] on a series of poly(macromonomer)s[31] (i.e., comblike polymers obtained by the polymerization of an oligomer containing a polymerizable chain end) having a PMMA backbone with

(27) TerMeer, H. U.; Burchard, W.; Wunderlich, W. *Colloid Polym. Sci.* **1980**, *258*, 675.

(28) Bantle, S.; Schmidt, M.; Burchard, W. *Macromolecules* **1982**, *15*, 1604.

(29) Wintermantel, M.; Gerle, M.; Fischer, K.; Schmidt, M.; Wataoka, I.; Urakawa, H.; Kajiwara, K.; Tsukahara, Y. *Macromolecules* **1996**, *29*, 978.

(30) Benoit, H.; Doty, P. *J. Phys. Chem.* **1953**, *57*, 958.

(31) (a) Percec, V.; Pugh, C.; Nuyken, O.; Pask, S. D. Macromonomers, Oligomers and Telechelics. in *Comprehensive Polymer Science*; Allen, G., Bevington, J. C., Eds.; Pergamon Press: Oxford, 1989; Vol. 6, pp 281−357. (b) *Macromonomer*: short name for *macro*molecular *monomer*, i.e., a polymer or oligomer containing a polymerizable group at one of its chain ends (ref 31a).

Table 2. Analysis of Polymers by XRD

polymer	T (°C)	d_{100} (Å)	d_{110} (Å)	d_{200} (Å)	$\langle d_{100}\rangle$ (Å)	a^a (Å)	R^b (Å)	S^c (Å)	ρ^d (g/cm^3)	μ^e
(*4*−*3,4*)12G1-CO_2CH_2PS	90	45.5	27.1	23.3	46.3	53.5	26.8	30.9	1.03	7.0
(*4*−*3,4,5*)10G1-CO_2CH_2PS	90	39.8	23.0	20.4	40.1	46.3	23.2	26.8	1.05	4.3
(*4*−*3,4,5*)12G1-CO_2CH_2PS	90	41.7	25.0	20.8	42.7	49.3	24.6	28.5	1.04	4.4
(*4*−*3,4,5*)12G1-CH_2PMA	85	39.9	22.9	19.7	39.7	45.6	22.9	26.4	0.96	3.7
(*4*−*3,4,5*)14G1-CO_2CH_2PS	90	44.2	26.4	22.7	45.1	52.1	26.1	30.1	1.02	4.5
(*4*−*3,4,5*)16G1-CO_2CH_2PS	90	49.0	28.8	24.1	49.0	56.6	28.3	32.7	1.01	4.9
(*4*−*3,4,5*)18G1-CO_2CH_2PS	90	52.0	30.5	25.3	51.8	59.8	29.9	34.5	0.99	5.0
(*3,4*−*3,4*)12G2-CO_2CH_2PS	90	47.0	27.1		47.0	54.2	27.1	31.3	0.99	4.7
(*3,4*−*3,5*)12G2-CO_2CH_2PS	90	41.7	24.5	21.2	42.2	48.8	24.4	28.2	0.99	3.8
(*3,4*−*3,4,5*)12G2-CO_2CH_2PS	90	41.7	24.4	20.8	41.9	48.4	24.2	27.9	0.99	2.6
(*3,4,5*−*3,4*)12G2-CO_2CH_2PS	90	38.4	22.8	20.0	39.3	45.4	22.7	26.2	0.98	2.5
(*3,4,5*−*3,5*)12G2-CO_2CH_2PS	90	34.8	20.8	18.3	35.9	41.4	20.7	23.7	0.98	2.1
(*3,4,5*−*3,5*)12G2-CH_2PMA	85	36.7	21.2	18.4	36.7	42.4	21.2	24.5	0.98	2.2
(*3,4,5*−*3,4,5*)12G2-CO_2CH_2PS	90	41.5	23.9	20.6	41.3	47.7	23.9	27.5	0.97	1.9
(*3,4,5*−*3,4,5*)12G2-CH_2PMA	85	42.3	24.5	42.1	42.3	48.8	24.4	28.2	0.98	1.9

[a] $a = 2\langle d_{100}\rangle/\sqrt{3}$. [b] $R = \langle d_{100}\rangle/\sqrt{3}$. [c] $S = 2R/\sqrt{3}$. [d] Density at 22 °C. [e] $\mu = (3\sqrt{3}N_A S^2\, t\rho)/2M$ = number of monomer units per column cross section with diameter a and height t = 3.74 Å. For detailed calculation, see ref 10.

Table 3. Comparison of Conformational Properties for Various Stiff Polymers

	solvent	M_n (rel, PS)	M_w/M_n (rel, PS)	M_w (abs, LS)	MW (monomer)	DP_{abs}	$R_{g,z}$[a] (Å)	R_h[b] (Å)	L[c] (Å)	a'[d] (Å)	l_k[e] (Å)	d[f] (Å)
Present Data												
Static /Dynamic LS												
(*4*−*3,4,5*)12G1-CO_2CH_2PS	THF	103 900	2.08	417 000	1 110	376	190	148	940	115	230	49.3
(*4*−*3,4,5*)12G1-CH_2PMA	THF	288 000	2.33	3 490 000	1 047	3 245	797	504	8 112	236	472	45.6
(*4*−*3,4,5*)12G1-CH_2PMA	toluene	288 000	2.33	3 270 000	1 047	3 039	740	475	7 598	216	432	45.6
SEC-MALLS												
(*4*−*3,4*)12G1-CO_2CH_2PS	THF	58 400	2.97		819					101	201	53.5
(*4*−*3,4,5*)10G1-CO_2CH_2PS	THF	127 000	2.71		1 025					159	317	46.3
(*4*−*3,4,5*)12G1-CO_2CH_2PS	THF	103 900	2.08		1 110					133	265	49.3
(*4*−*3,4,5*)12G1-CH_2PMA	THF	288 000	2.33		1 047		711	433		237	474	45.6
(*4*−*3,4*)16G1-CO_2CH_2PS	THF	114 600	2.57		1 278					223	445	56.6
(*3,4*−*3,4*)12G2-CO_2CH_2PS	THF	148 900	2.28		1 194					198	395	54.2
(*3,4,5*−*3,4,5*)12G2-CO_2CH_2PS	THF	119 600	2.02		2 216					363	725	47.7
(*3,4,5*−*3,4,5*)12G2-CH_2PMA	THF	227 700	3.11		2 154					516	1 032	48.8
Schmidt[g]												
KPS800MA1730	toluene			1 500 000	800	1 875.0	430		4 688		261	
BPS1000MA903	toluene			894 000	1 000	894.0	257		2 235		232	
BPS1700MA1867	toluene			3 100 000	1,700	1 823.5	477		4 559		390	
KPS2900MAY	toluene				2 900						890	
BPS3900MAY	toluene				3 900						1 280	
BPS4000MA602	toluene			2 380 000	4 000	595.0	400		1 488		1 280	
BPS5000MA547	toluene			2 700 000	5 000	540.0	447		1 350		2 076	
KPS5500MAY	toluene				5 500							
Schlueter[h]												
6(G2) 82k	toluene			213 000	875	243	150					
6(G2) 600k	toluene			2 140 000	875	2 446	400		6 114	80[i]	160[i]	

[a] Radius of gyration. [b] Hydrodynamic radius. [c] Contour length. [d] Persistence length. [e] Kuhn segment length. [f] Column diameter. [g] Data from ref 29. [h] Data from ref 34. [i] Recalculated values for the data reported in ref 29.

oligostyrene side chains. Since the **(*4*−*3,4,5*)12G1-CH_2PMA** specimen studied in the present work has a very high degree of polymerization of its PMMA backbone, the value of its R_g is determined by the conformation of the PMMA backbone and, therefore, is influenced only indirectly by the structure and molecular weight of the pendant side groups (i.e., the cross-sectional dimension of the polymer does not contribute to the overall R_g). Thus, we expect that there should be a close correlation between R_g values for PMA and PS chains with monodendritic side groups and those reported by Wintermantel et al.[29] Analogous observations were made in earlier light-scattering studies of very high molecular weight mucin glycoproteins[32,33] which consist of a linear polypeptide backbone, heavily substituted with oligosaccharide side groups. A universal scaling of the R_g values was found with regard to the molecular weight of the protein backbone, independent of the side-chain molecular weight, provided the side groups were longer than disaccharides.[32,33] This observation was consistent with conformational energy calculations,[33] which showed that, because of steric interactions between the polypeptide backbone and the sugar side groups, the backbone becomes highly extended.

Wintermantel et al.[29] found that the Kuhn segment length increased systematically, as the oligostyrene side groups' length increased. For **(*4*−*3,4,5*)12G1-CH_2PMA**, our result, l_k = 474 Å, seems quite consistent numerically with values determined by Wintermantel et al.[29] for poly(macromonomer)s based on a PMA backbone and PS side groups, which range from l_k = 230 (side group with MW = 990) to 2080 Å (side group with MW = 4940). Our results indicate a stiffness intermediate

(32) Shogren, R. L.; Jamieson, A. M.; Blackwell, J.; Jentoft, N. *Biopolymers* **1986**, *25*, 1505.

(33) Shogren, R. L.; Gerken, T.; Jentoft, N. *Biochemistry* **1989**, *28*, 5525.

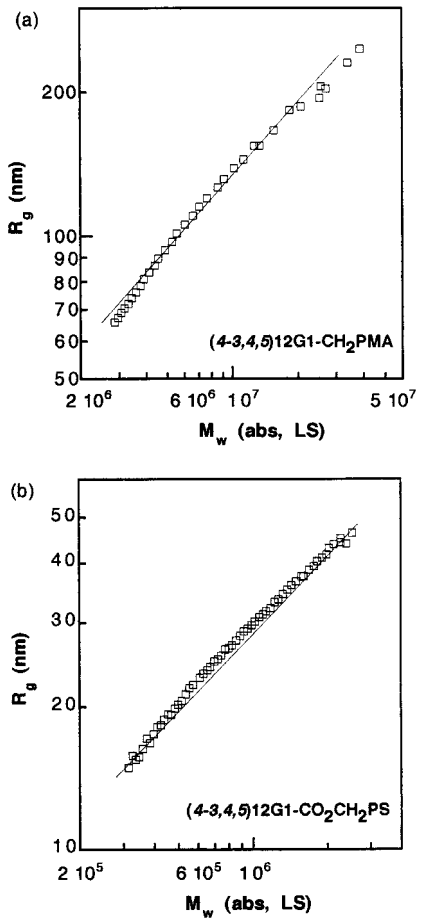

Figure 4. Dependence of radius of gyration (R_g) on M_w(abs, LS) of (a) **(*4*−*3,4,5*)12G1-CH$_2$PMA** and (b) **(*4*−*3,4,5*)12G1-CO$_2$CH$_2$PS** (see Experimental Section and ref 26b for calculations).

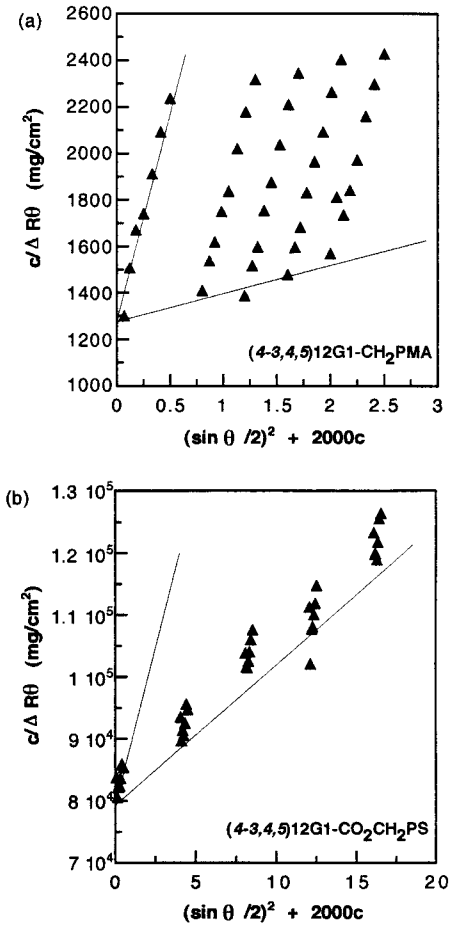

Figure 5. Zimm plot for (a) **(*4*−*3,4,5*)12G1-CH$_2$PMA** and for (b) **(*4*−*3,4,5*)12G1-CO$_2$CH$_2$PS** in THF at 25 °C (see Experimental Section and ref 26b for calculations).

between that obtained by Wintermantel et al.[29] for poly(macromonomer)s with oligostyrene side groups of MW = 1740 and 2740, respectively.

Next, we contrast our results for **(*4*−*3,4,5*)12G1-CO$_2$CH$_2$PS** with the light-scattering data of Neubert et al.[34] on polystyrenes with Fréchet-type dendritic side groups. These polymers do not self-organize in a lattice. For a fractionated polymer, having a second generation Fréchet-type monodendritic pendent group, these authors determined M_w(abs, LS) = 2.14 × 10^6, $R_{g,z}$ = 400 Å, and R_h = 280 Å. Reinterpreting their results by crudely applying the wormlike chain model assuming a Schultz−Flory chain length distribution[1a] (eq 1), their data yield values for l_k between 100 and 200 Å (i.e., 100 Å for high M_w, 200 Å for low M_w sample). These results are not corrected for polydispersity (unreported in ref 34) and, therefore, are overestimated. Returning to Figure 5b, for **(*4*−*3,4,5*)12G1-CO$_2$CH$_2$PS**, we find l_k = 265 Å, i.e., 1.7 times larger than the recalculated result of Neubert et al.[34] for a PMMA with second generation Fréchet-type monodendritic side groups.

Following the above discussion, it is interesting to compare R_g values for different monodendron side groups attached to PS and PMMA backbones. First, in Figure 7a, we plot R_g data for different PS against the degree of polymerization DP$_{abs}$, using only SEC-MALLS analyses in the range of molecular weight where the anomaly was least pronounced. We see a clear trend in which, for a given DP$_{abs}$, R_g values fall in decreasing order **(*3,4,5*−*3,4,5*)12G2-CH$_2$PMA** > **(*3,4,5*−*3,4,5*)12G2-CO$_2$CH$_2$PS** > **(*3,4*−*3,4,5*)12G2-CO$_2$CH$_2$PS** > **(*3,4*−*3,5*)12G2-CO$_2$CH$_2$PS** > **(*4*−*3,4,5*)12G1-CO$_2$CH$_2$PS** > **(*4*−*3,4*)12G1-CO$_2$CH$_2$PS**. This order correlates to the solid-state chain conformations observed via X-ray diffraction (Chart 3), for which the $l_{monomer}$ values are listed in Table 4 and the μ values in Chart 3. This trend is also in agreement with that of the plateau of the Φ_h isotropization temperature from Figure 2. Considering polymers with a PS backbone, Table 4 and Figure 7 indicate that the chain with the **(*3,4,5*−*3,4,5*)12G1-** substituent has the largest $l_{monomer}$ and the largest R_g, whereas the chain with the **(*4*−*3,4*)12G1-** substituent has the smallest $l_{monomer}$ and the smallest R_g. This suggests analogous conformation-directing influences of the substituent in solid state and solution. However, application of the wormlike chain model to the experimental R_g values using $l_{monomer}$ values obtained from X-ray diffraction analysis yields too large values for the persistence length (Table 4). In addition, contrasting **(*3,4,5*−*3,4,5*)12G2-CO$_2$CH$_2$PS** and **(*3,4,5*−*3,4,5*)-12G2-CH$_2$PMA**, chains with identical substituents but different backbones, we find from Table 4 and Figure 7b that, although $l_{monomer}$ from X-ray diffraction is the same for each chain, R_g is larger for the **PMA** backbone. The latter result agrees with our above light-scattering analysis of R_g data for **(*4*−*3,4,5*)-12G1-CH$_2$PMA** and **(*4*−*3,4,5*)12G1-CO$_2$CH$_2$PS** via eq 1, which yields l_k = 474 and 265 Å, respectively. Thus, it appears that there are substantial differences between the solid-state and solution conformations such that the extension of the PMA backbone is larger. SFM experiments will access a comparative study of these polymers in solution and in disordered and ordered solid states.

(34) Neubert, I.; Amoulong-Kirstein, E.; Schlüter, A.-D.; Dautzengerg, H. *Macromol. Rapid Commun.* **1996**, *17*, 517.

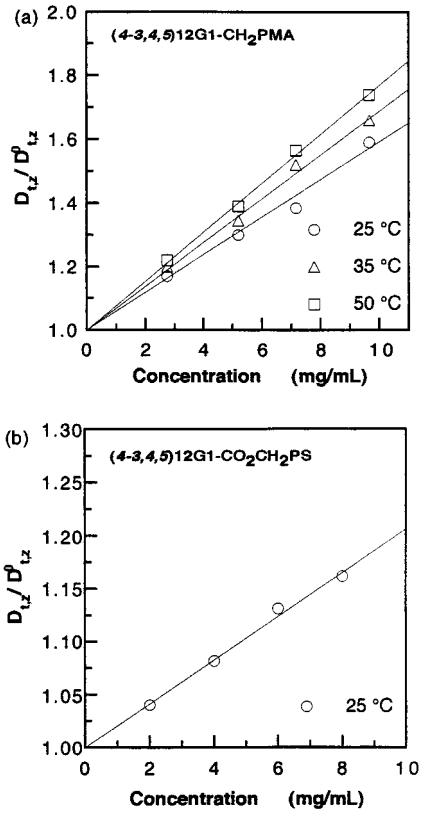

Figure 6. Concentration dependence of normalized diffusion coefficient in THF for (a) **(*4*−*3,4,5*)12G1-CH$_2$PMA** and for (b) **(*4*−*3,4,5*)12G1-CO$_2$CH$_2$PS** (see Experimental Section and ref 26b for calculations).

Structural Analysis by Direct Visualization of Individual Cylindrical Polymers by SFM. In a preliminary communication,[6] we reported preliminary results on the imaging by SFM of monolayers of spherical (below $DP_{abs} = 20$) and respectively cylindrical (above $DP_{abs} = 20$) polymers obtained from **(*3,4,5*−*3,4,5*)12G2-CO$_2$CH$_2$PS** with different degrees of polymerization (DP_{abs}) on mica. The diameter of the spherical and cylindrical polymers (50 ± 5 Å) determined by SFM was in very good agreement with the corresponding values obtained by XRD when the same polymers were self-organized in a Pm$\bar{3}$n cubic (diameter of 46.3 Å) and p6mm Φ_h (diameter of 47.7 Å) lattice and was in the range required for quantitative analysis by visualization.[2,3] Since the order in the monolayer is closer to an isotropic state than to a lattice, these results suggest that the cylindrical shape of these macromolecules may persist in both ordered and disordered states.

Figure 8 presents several representative examples of direct visualization of individual cylindrical macromolecules **(*4*−*3,4,5*)14G1-CO$_2$CH$_2$PS** (M_w(abs, LS) = 990 000) and **(*3,4,5*−*3,4,5*)12G2-CH$_2$PMA** (M_w(abs, LS) = 1 110 000) on the surface of a highly ordered pyrolitic graphite (HOPG). The conformation of **(*4*−*3,4,5*)14G1-CO$_2$CH$_2$PS** is influenced by some interactions with HOPG substrate (template effect), which induce straight segments that are bent at angles of 60° and 120°, corresponding to the three fold symmetry of the graphite substrate. This template effect is not observed for the case of **(*3,4,5*−*3,4,5*)12G2-CH$_2$PMA**. The number of the single chains on a surface, i.e., the coverage of the substrate, could be manipulated by the concentration of the solution from which the film was spincast at 21 °C with 2000 rpm (c = 0.06 mg/mL in Figure 8a and c = 0.10 mg/mL in Figure 8c). Individual macromolecules were visualized when films were cast from very dilute solution (Figure 8a). By analogy with the analysis of the complexes of DNA with proteins,[2,3] the overlay and underlay at crossing points of **(*4*−*3,4,5*)14G1-CO$_2$CH$_2$PS** and **(*3,4,5*−*3,4,5*)12G2-CH$_2$PMA** chains and the contacts between their chain ends could be determined from a detailed examination of Figure 8a and d. This allowed the direct determination of both diameter and contour length of these macromolecules.

The weight-average contour length measured by SFM ($L_{w,SFM}$ = 1200 Å) and averaged for almost 200 chains of **(*3,4,5*−*3,4,5*)12G2-CH$_2$PMA** corresponds to a monomer length $l_{monomer}$ = 2.3 Å, comparable to that for the fully extended all-trans polymethacrylate backbone, $l_{monomer}$ = 2.5 Å, and somewhat larger than the value obtained from XRD in the Φ_h mesophase, $l_{monomer}$ = 1.97 Å. The situation is different for the case of **(*4*−*3,4,5*)14G1-CO$_2$CH$_2$PS**, where the backbone is jacketed with less bulkier monodendritic side-groups. The weight-average contour length of **(*4*−*3,4,5*)14G1-CO$_2$CH$_2$PS** measured by SFM ($L_{w,SFM}$ = 1020 Å) corresponds to $l_{monomer}$ = 1.2 Å, much smaller than the fully extended all-trans polystyrene value, $l_{monomer}$ = 2.5 Å, but larger than the value obtained in the Φ_h phase via XRD, $l_{monomer}$ = 0.83 Å. These observations are again consistent with the SEC-MALLS data in Figure 7, which show that the radius of gyration of **(*3,4,5*−*3,4,5*)12G2-CH$_2$PMA** is considerably larger than that of **(*4*−*3,4,5*)14G1-CO$_2$CH$_2$PS** at comparable DP values, also reflected in the larger value of the Kuhn segment length of the former (Table 4). This demonstrates that the increased stiffness of the polymer backbone induced by the bulkier dendritic side chain of **(*3,4,5*−*3,4,5*)-12G2-CH$_2$PMA** compared to that of **(*4*−*3,4,5*)14G1-CO$_2$CH$_2$PS** is manifested in the ordered Φ_h solid state (larger $l_{monomer}$), the disordered surface state (increased $L_{w,SFM}$) and the solution state (larger R_g and l_k) (Figure 7, Tables 3 and 4).

Thus, three different sets of experiments demonstrate that the contour length of **(*3,4,5*−*3,4,5*)12G2-CH$_2$PMA** is substantially larger than that of **(*4*−*3,4,5*)14G1-CO$_2$CH$_2$PS** and that it changes very little at the transition from the Φ_h 2-D ordered lattice (determined by XRD) to the solid state on a surface (SFM). **(*3,4,5*−*3,4,5*)12G2-CH$_2$PMA** shows about a 15% extension on the surface state, whereas **(*4*−*3,4,5*)14G1-CO$_2$CH$_2$PS** shows about 45% extension. Light-scattering measurements of R_g indicate that similar conformations to these surface states are present in solution. Our observations provide definitive evidence that backbone stiffening can be induced by coating with dendritic side groups.[6] Attachment of the monodendritic side group **(*3,4,5*−*3,4,5*)12G2-** both to PMA and to PS stiffens these backbones by producing an almost fully extended chain conformation in ordered and disordered solid states and in solution. In contrast, in all three states, attachment of the less bulky monodendritic side group **(*4*−*3,4,5*)14G1-** permits a substantially more contracted conformation. These results confirm that we have prepared the first library of polymers with controlled chain conformation and stiffness which can be quantitatively analyzed via direct visualization.

Figure 8b shows the SFM picture of the film from Figure 8a after annealing for 20 h at 21 °C. During annealing, the individual chains from Figure 8a moved, came together, and segregated in an ordered layer. This preliminary experiment demonstrates that direct visualization of these synthetic macromolecular chains provides a tool to investigate the mechanism of order formation at the molecular level in two dimensions, starting from individual disordered macromolecules. Although the HOPE substrate templates the polymer chain conformation, it does allow a quantitative analysis of its contour length, diameter end-to-end contacts, and overlay of the crossings.

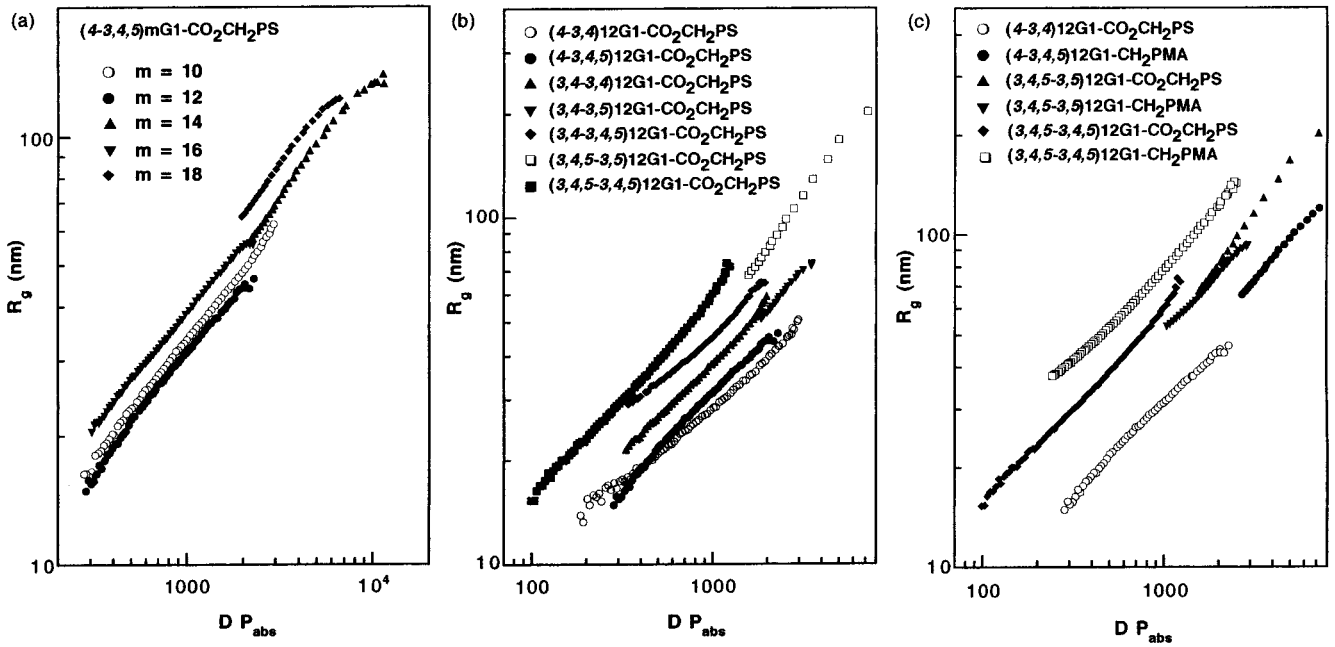

Figure 7. Dependence of radius of gyration (R_g) on DP_{abs} for the library of polymers with monodendritic side groups: (a) **(*4*−*3,4,5*)mG1-CO_2CH_2PS** (m = 10, 12, 14, 16, 18); (b) PS with different monodendritic side groups; (c) comparison between PS and PMA with identical monodendritic side groups.

Table 4. Monomer Length in the Φ_h Phase and Kuhn Segment Length (l_k) in Solution

polymer	$l_{monomer}$[a] (Å)	l_k[b] (Å)	l_k[c] (Å)
(*4*−*3,4*)12G1-CO_2CH_2PS	0.53	980	201
(*4*−*3,4,5*)10G1-CO_2CH_2PS	0.87	770	317
(*4*−*3,4,5*)12G1-CO_2CH_2PS	0.85	670	265
(*4*−*3,4,5*)10G1-CH_2PMA	0.83	1290	474
(*4*−*3,4,5*)14G1-CO_2CH_2PS	0.83	1250	415[d]
(*4*−*3,4,5*)16G1-CO_2CH_2PS	0.76	1160	445
(*4*−*3,4,5*)18G1-CO_2CH_2PS	0.75	1890	567[d]
(*3,4*−*3,4*)12G2-CO_2CH_2PS	0.80	1120	395
(*3,4*−*3,5*)12G2-CO_2CH_2PS	0.98	910	357[d]
(*3,4*−*3,4,5*)12G2-CO_2CH_2PS	1.44	920	530[d]
(*3,4,5*−*3,5*)12G2-CO_2CH_2PS	1.78	1300	926[d]
(*3,4,5*−*3,5*)12G2-CH_2PMA	1.70	940	640[d]
(*3,4,5*−*3,4,5*)12G2-CO_2CH_2PS	1.97	920	725[d]
(*3,4,5*−*3,4,5*)12G2-CH_2PMA	1.97	1310	1032[d]

[a] Calculated from XRD. [b] Calculated by eq 1 assuming $l_{monomer}$ is the same as in the Φ_h phase. [c] Assuming $l_{monomer}$ = 2.5 Å. [d] Calculated by eq 1.

Experiments with other substrates (to be reported soon) do not provide any template effect. The detection and identification of individual molecules and macromolecules by visualization via various techniques represents and extremely active field of research.[35] With very few exceptions,[35c] all previous experiments were accomplished on 2-D crystals.[35a,b,d] However, the quantitative analysis of synthetic polymers with different stiffness, architecture, and topology in different ordered and disordered states at the level of resolution achieved on complexed DNA[2,3] becomes accessible with the present class of cylindrical polymers.

Two additional examples of cylindrical macromolecules obtained by coating polymer backbones with monodendritic building blocks were recently reported from two other laboratories.[36] However, they do not exhibit the degree of perfection needed to pack into a lattice that can be characterized by XRD, nor do they exhibit the synthetic capabilities of this monodendritic library of monomers and polymers, i.e., extremely fast and controlled polymerization by a conventional radical initiation process.[16]

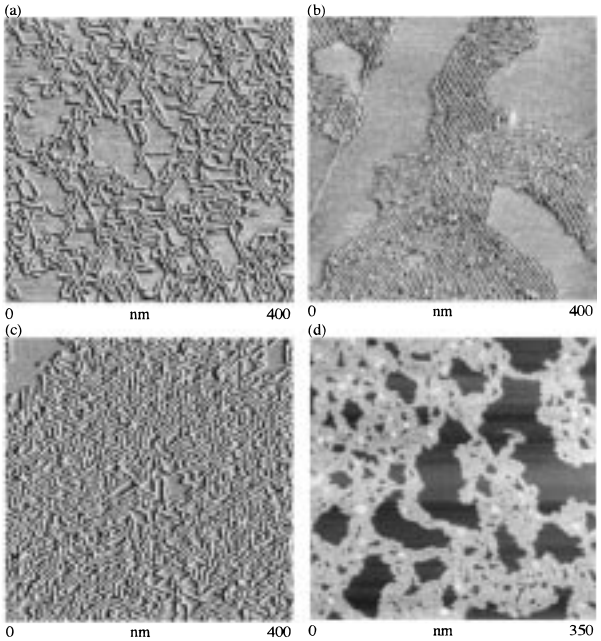

Figure 8. Direct visualization of individual cylindrical macromolecules by SFM on the surface of highly ordered pyrolitic graphite (HOPG). Samples were prepared from cyclopentane solution by spin-casting at 21 °C with 2000 rpm: (a) **(*4*−*3,4,5*)14G1-CO_2CH_2PS**, c = 0.06 mg/mL; (b) after annealing (a) at 70 °C for 20 h; (c) **(*4*−*3,4,5*)14G1-CO_2CH_2PS**, c = 0.10 mg/mL; (d) **(*3,4,5*−*3,4,5*)12G_2-CH_2PMA**, c = 0.06 mg/mL.

(35) (a) Fromer, J. *Angew. Chem., Int. Ed. Engl.* **1992**, *31*, 1298. (b) Walba, D. M.; Stevens, F.; Clark, N. A.; Parks, D. C. *Acc. Chem. Res.* **1996**, *29*, 591. (c) Jung, T. A.; Schlittler, R. R.; Gimzewski, J. K. *Nature (London)* **1997**, *386*, 696. (d) Grim, P. C. M.; DeFeyter, S.; Gesquiere, A.; Vanoppen, P.; Rücker, M.; Valiyaveettil, S.; Moessner, G.; Müllen, K.; De Schryver, F. C. *Angew. Chem., Int. Ed. Engl.* **1997**, *36*, 2601.

(36) (a) Tomalia, D. A.; Kirchoff, P. M. U.S. Patent 4,694,064, 1987. (b) Yin, R.; Zhu, Y.; Tomalia, D. A.; Ibuki, H. *J. Am. Chem. Soc.* **1998**, *120*, 2678. (c) Karakaya, B.; Claussen, W.; Gessler, K.; Saenger, W.; Schlüter, A.-D. *J. Am. Chem. Soc.* **1997**, *119*, 3296.

Conclusions

A library containing 13 self-assembling first and second generation monodendrons was synthesized, characterized, and used in the preparation of a library of 16 styrene and methacrylate monodendritic monomers and their corresponding polymers. Fifteen of these polymers exhibit a well-defined cylindrical shape that self-organizes in a Φ_h 2-D LC lattice. Analysis of this lattice by XRD produced information on the cylinder diameter, which varies from 60 to 41 Å, and on the number of monodendritic repeat units forming the cylinder stratum (μ). The value of μ can be systematically varied from 7 to 1.9. Since the backbone of these cylindrical polymers passes through their center, for a particular backbone the value of μ can change its conformation from helical to fully extended. At the same time, the stiffness of the polymer increases. Dynamic and static light-scattering experiments have demonstrated a similar trend for the stiffness of these polymers in solution. The large diameter of these polymers allowed the direct visualization of single chains and of monolayers of these cylindrical macromolecules on a surface and their quantitative analysis. The contour length of the individual chains of the most rigid polymer determined by SFM was compared with its contour length from light-scattering and XRD experiments. The agreement between these values demonstrates the validity of our research hypothesis and generates a new mechanism to manipulate systematically and in a predictive way the properties of polymers obtained from backbones coated with libraries of self-assembling monodendrons. Direct visualization of these cylindrical macromolecules combined with manipulation of their structure at the angstrom level[18] opens new opportunities for the field of synthetic macromolecules with well-defined shapes and nanometer-scale dimensions. The study of the larger generations of monodendritic monomers from this library, the reversible jacketing of polymers with these monodendrons via nonbonding interactions,[37] and the investigation of self-organization of polymeric materials by direct visualization using the library of polymers described here are in progress.

Experimental Section

General Methods. ^{1}H (200 MHz) and ^{13}C (50 MHz) NMR spectra were recorded on a Varian Gemini 200 spectrometer with tetramethylsilane (TMS) as internal standard. Elementary analysis was performed at MHW laboratories in Phoenix, AZ. The purity of products was determined by a combination of thin-layer chromatography (TLC) on silica gel plates (Kodak) with fluorescent indicator and high-pressure liquid chromatography (HPLC) using a Perkin-Elmer series 10 high-pressure liquid chromatograph equipped with an LC-100 column oven, Nelson Analytical 900 series integrator data station, and two Perkin-Elmer PL gel columns of 5×10^2 and 1×10^4 Å. THF was used as solvent. Detection was by UV absorbance at 254 nm. Relative molecular weights were determined by reference to polystyrene standards by using the same instrument and a set of columns of 10 μm, 500 Å and 10 μm, 10^4 Å. Thermal transitions were measured on a Perkin-Elmer DSC-7 differential scanning calorimeter. In all cases, the heating and cooling rates were 10 °C min^{-1}. The transition temperatures were reported as the maxima and minima of their endothermic and exothermic peaks. Indium was used as calibration standard. An Olympus BX-40 optical polarized microscope (100× magnification) equipped with a Mettler FP 82 hot stage and a Mettler FP 80 central processor was used to verify thermal transitions and characterize anisotropic textures.

X-ray diffraction (XRD) patterns were recorded using either a helium-filled flat plate wide-angle (WAXS) camera or a pinhole-collimated small-angle (SAXS) camera, and also by an Image Plate area detector (MAR Research) with a graphite-monochromatized pinhole-collimated beam and a helium tent. Small-angle diffraction (SAXD) from powder specimen was recorded with a quadrant detector at station 8.2 of the Synchrotron Radiation Source at Daresbury, UK. The samples, in glass capillaries, were held in a temperature-controlled cell (±0.1 °C). The beampath up to the beamstop was either evacuated or flushed with N_2. Ni-filtered Cu Kα radiation was used. Densities (ρ_{20}) were determined by flotation in gradient columns at 20 °C.

Size exclusion chromatography multiangle light-scattering (SEC-MALLS) experiments were performed with THF as eluent at a flow rate of 1 mL/min. The concentrations of the injected solutions were in the range of 1−4 g/L. The refractive index increment was 0.172. LS measurements were done every 4 s at 20 different angles with a MALLS detector ALV-1800. The light source was an Ar ion laser 2017 from Spectra Physics. A Waters W410 (RI detector) was used as the concentration detector. GPC gel columns from PSS Mainz (5 μm, 10^6, 10^5, 10^3 Å) were used for the separation of the polymer samples. Static and dynamic light-scattering measurements were carried out with equipment from a Brookhaven Instruments with a 5-mW He/Ne laser, a goniometer with refractive index matching bath, and a photomultiplier tube. The specific refractive index, dn/dc, was measured using a Brice-Phoenix differential refractometer (C. N. Woods, State College, PA) and calibrated against NaCl−H_2O mixtures. The dn/dc value of **(*4*−*3,4,5*)12G1-CH$_2$PMA**/THF solution was found to be dn/dc = 0.172 mL/g, and that of **(*4*−*3,4,5*)12G1-CH$_2$PMA**/toluene solution was 0.153 mL/g at 20 °C and λ = 632.8 nm. Values of the excess Rayleigh's ratios (ΔR) of the solutions were determined by calibration against benzene.

Solutions of **(*4*−*3,4,5*)12G1-CO$_2$CH$_2$PS** in THF and **(*4*−*3,4,5*)-12G1-CH$_2$PMA** in THF and toluene for light-scattering experiments were made by dissolving weighted quantities (Perkin-Elmer microbalance, model AD-2, with an accuracy of 0.1 μg) in a known volume of filtered solvent (0.22 μm Millipore filters). Stock solutions were equilibrated for 48 h with intermittent shaking. Dilutions were made on a volumetric basis, by addition of known amounts of filtered solvent. For light-scattering measurements, solutions were passed through 0.22 μm filters directly into dust-free light-scattering cells, which were sealed and centrifuged at 5000 rpm for 30 min prior to experimental analysis. All solutions were checked for optical clarity and absence of dust particles by monitoring the scattering intensity for 50−75 runs of 1 s duration. Solutions used for light-scattering study were those which had fluctuations in scattered intensity of less than 3%. Since THF was found to be a very good solvent for **(*4*−*3,4,5*)12G1-CH$_2$PMA** and **(*4*−*3,4,5*)12G1-CO$_2$CH$_2$PS**, the concentration extrapolations of excess Rayleigh's ratios were performed by square-root plots,

$$(Kc/\Delta R(c,\theta))^{1/2} = (Kc/\Delta R(0,\theta))^{1/2}(1 + A_2 M_w^{app} c) \qquad (2)$$

and the extrapolated values of $Kc/\Delta P(0,\theta)$ were analyzed by a Zimm plot,[26b]

$$Kc/\Delta R(0,\theta) = (1/M_w)(1 + q^2 R_{g,z}{}^2/3) \qquad (3)$$

Here, the scattering vector, $q = (4\pi n/\lambda) \sin \theta/2$, where n is refractive index, λ is the wavelength of incident light, and θ is scattering angle. The analysis yields the weight-average molecular weight, M_w(abs, LS), the z-average of the squared radius of gyration,[1e,8c,26b] $R_{g,z}{}^2$, and the second osmotic virial coefficient, A_2. Dynamic light-scattering data were analyzed by the method of cumulants to yield the z-average translational diffusion coefficient, $D_{t,z}$, from the first cumulant. Extrapolation of $D_{t,z}$ to zero concentration enables us to obtain the hydrodynamic radius, R_h, via the Stokes−Einstein equation,[1e,26b]

$$D_{t,z}{}^0 = kT/6\pi\eta R_h \qquad (4)$$

where k is Boltzmann's constant, T is absolute temperature, and η is solvent viscosity. From the second cumulant, μ_2, we obtain a measure of the polydispersity in size distribution.

(37) (a) van Nunen, J. L. M.; Folmer, B. F. B.; Nolte, R. J. M. *J. Am. Chem. Soc.* **1997**, *119*, 283. (b) Beijer, F. H.; Kooijman, H.; Spek, A. L.; Sijbesma, R. P.; Meijer, E. W. *Angew. Chem., Int. Ed. Engl.* **1998**, *37*, 75.

Scanning force microscopy measurements were performed with a Nanoscope III (Digital Instruments, Santa Barbara, CA) operating in the tapping mode at a resonance frequency of ∼360 Hz and using Si probes with a spring constant of ∼50 N/m. Tips having an apex radius below 10 nm were selected by means of a special calibration standard. A sharp apex was essential in order to resolve the relatively soft molecules of about 5 nm in diameter. Measurements were done at ambient conditions, i.e., in air at 21 °C. Samples for the SFM experiments were prepared by spin-casting of dilute cyclopentane solutions with concentration varying from 0.1 to 0.01 mg/mL. The spin-coating was done at room temperature at 2000 rpm on pyrolytic graphite as a substrate. Depending on the concentration, different degrees of the substrate coverage were obtained.

Acknowledgment. Financial support by the National Science Foundation (DMR-97-08581), Deutsche Forschungsgemeinschaft, Engineering and Physical Science Research Council (UK), and a Humboldt Research Award for Senior US Scientists to V.P. is gratefully acknowledged.

Supporting Information Available: Four reaction schemes describing the synthesis of monodendritic monomers and experimental details of their synthesis, analytical data, and references (59 pages, print/PDF). See any current masthead page for ordering information and Web access instructions.

JA981211V